JGR Planets

RESEARCH ARTICLE
10.1029/2020JE006382

Special Section:
InSight at Mars

A New Crater Near InSight: Implications for Seismic Impact Detectability on Mars

I. J. Daubar[1], P. Lognonné[2], N. A. Teanby[3], G. S. Collins[4], J. Clinton[5], S. Stähler[6], A. Spiga[7], F. Karakostas[8], S. Ceylan[6], M. Malin[9], A. S. McEwen[10], R. Maguire[8], C. Charalambous[4], K. Onodera[2], A. Lucas[2], L. Rolland[11], J. Vaubaillon[12], T. Kawamura[2], M. Böse[5], A. Horleston[3], M. van Driel[6], J. Stevanović[13], K. Miljković[14], B. Fernando[15], Q. Huang[16], D. Giardini[6], C. S. Larmat[17], K. Leng[15], A. Rajšić[14], N. Schmerr[8], N. Wójcicka[4], T. Pike[4], J. Wookey[3], S. Rodriguez[2], R. Garcia[18], M. E. Banks[19], L. Margerin[20], L. Posiolova[9], and B. Banerdt[21]

[1]Department of Earth, Environmental, and Planetary Sciences, Brown University, Providence, RI, USA, [2]Université de Paris, Institut de physique du globe de Paris, CNRS, Paris, France, [3]School of Earth Sciences, University of Bristol, Wills Memorial Building, Queens Road, Bristol, UK, [4]Department of Earth Science and Engineering, Imperial College London, South Kensington Campus, London, UK, [5]Swiss Seismological Service (SED), ETH Zurich, Zurich, Switzerland, [6]Institute of Geophysics, ETH Zürich, Zürich, Switzerland, [7]Laboratoire de Météorologie Dynamique/Institut Pierre Simon Laplace (LMD/IPSL), Sorbonne Université, Centre National de la Recherche Scientifique (CNRS), École Polytechnique, École Normale Supérieure (ENS), Campus Pierre et Marie Curie BC99, Paris, France, [8]Department of Geology, University of Maryland, College Park, College Park, MD, USA, [9]Malin Space Science Systems, San Diego, CA, USA, [10]Lunar and Planetary Laboratory, University of Arizona, Tucson, AZ, USA, [11]Université Côte d'Azur, Observatoire de la Côte d'Azur, CNRS, IRD, Valbonne, France, [12]Observatoire de Paris, IMCCE, PSL, Paris, France, [13]AWE Blacknest, Aldermaston, Reading, UK, [14]Space Science and Technology Centre, School of Earth and Planetary Sciences, Curtin University, Perth, WA, Australia, [15]Department of Earth Sciences, University of Oxford, Oxford, UK, [16]Department of Geology, University of Maryland, College Park, MD, USA, [17]Los Alamos National Laboratory, Los Alamos, NM, USA, [18]Institut Supérieur de l'Aéronautique et de l'Espace SUPAERO, Toulouse, France, [19]NASA Goddard Space Flight Center, Greenbelt, MD, USA, [20]Institut de Recherche en Astrophysique et Planétologie, Université Toulouse III Paul Sabatier, CNRS, CNES, Toulouse, France, [21]Jet Propulsion Laboratory, California Institute of Technology, Pasadena, CA, USA

Key Points:
- A new 1.5 m diameter impact crater formed on Mars ~40 km from the InSight lander between February and April 2019
- Three candidate seismic events occurred during this time frame, but none of them can be definitively associated with the new crater
- We revise our expectations for InSight impact detections above the background noise to be ~2 per Earth year, with large uncertainties

Supporting Information:
- Supporting Information S1

Correspondence to:
I. J. Daubar,
ingrid_daubar@brown.edu

Citation:
Daubar, I. J., Lognonné, P., Teanby, N. A., Collins, G. S., Clinton, J., Stähler, S., et al. (2020). A new crater near InSight: Implications for seismic impact detectability on Mars. *Journal of Geophysical Research: Planets*, *125*, e2020JE006382. https://doi.org/10.1029/2020JE006382

Received 14 JAN 2020
Accepted 2 JUL 2020
Accepted article online 11 JUL 2020

Abstract A new 1.5 m diameter impact crater was discovered on Mars only ~40 km from the InSight lander. Context camera images constrained its formation between 21 February and 6 April 2019; follow-up High Resolution Imaging Science Experiment images resolved the crater. During this time period, three seismic events were identified in InSight data. We derive expected seismic signal characteristics and use them to evaluate each of the seismic events. However, none of them can definitively be associated with this source. Atmospheric perturbations are generally expected to be generated during impacts; however, in this case, no signal could be identified as related to the known impact. Using scaling relationships based on the terrestrial and lunar analogs and numerical modeling, we predict the amplitude, peak frequency, and duration of the seismic signal that would have emanated from this impact. The predicted amplitude falls near the lowest levels of the measured seismometer noise for the predicted frequency. Hence, it is not surprising this impact event was not positively identified in the seismic data. Finding this crater was a lucky event as its formation this close to InSight has a probability of only ~0.2, and the odds of capturing it in before and after images are extremely low. We revisit impact-seismic discriminators in light of real experience with a seismometer on the Martian surface. Using measured noise of the instrument, we revise our previous prediction of seismic impact detections downward, from ~a few to tens, to just ~2 per Earth year, still with an order of magnitude uncertainty.

Plain Language Summary A small new impact crater was discovered on Mars very close to the InSight lander. Photographs from a camera in orbit show it formed between 21 February and 6 April 2019. Three seismic events were detected by InSight during this time. We estimate what seismic data from the impact would have looked like and whether or not each of the seismic events was caused by the new impact, but none of them can be definitely linked. We predict the size, frequency, and length of time of the signal that would have come from this impact. Even though this impact is very close to InSight, it is small, so it was not a large seismic event. The signal would be near the quietest the instrument ever gets. There is only a 1 in 5 chance each Earth year that a crater would have formed this close to InSight, and a much lower chance

that it would be imaged; thus, we were very lucky to find this crater. Using what we know about the instrument on the ground, we update the number of impacts we expect to find with InSight to ~2 each Earth year, with a lot of uncertainty.

1. A New Impact Constrained by Orbital Images

On 6 April 2019, an image taken by the Context camera (CTX; Malin et al., 2007) on the Mars Reconnaissance Orbiter revealed a new dark spot that was not present in a previous image taken on 21 February (Figure 1), only ~40 km from the newly landed InSight mission (Interior Exploration using Seismic Investigations, Geodesy, and Heat Transport; Smrekar et al., 2019). Detecting an impact in both seismic data and orbital images would be an exciting development, leading to a number of scientific advances (Daubar et al., 2018). This would be a seismic source with a known location and, thus, a known distance and direction. A certain location and depth would allow modeling of seismic ray paths through the interior that could constrain seismic velocities and the physical properties of the material through which the rays traveled. This would improve models of interior structure and the seismic attenuation of Mars. An impact clearly observed in both orbital and seismic data would also provide a calibration of the seismic source parameters such as moment, cutoff frequency, and seismic efficiency (the ratio of impact energy to radiated seismic energy). The seismic efficiency, for example, is not well constrained, with values in the literature ranging from 10^{-6} to 10^{-2} (Daubar et al., 2018, and references therein). High resolution images of newly formed craters would characterize crater sizes, leading to an empirical relationship between impact size and observed seismic amplitudes. Enough such observations would also result in an independent measurement of the current impact rate, anchoring absolute bombardment rates. Thus, identifying an impact in seismic data that was also imaged from orbit would satisfy many important scientific goals. So naturally, this event was of immediate interest to the InSight team.

A high-resolution 25 cm pixel scale image from the High Resolution Imaging Science Experiment (HiRISE; McEwen et al., 2007) was acquired shortly thereafter. The HiRISE image resolved a ~1.5 m diameter impact crater at the location of the new dark spot (Figure 1d), showing that an impact event occurred in the short period of time constrained by the before and after CTX images, between 21 February (03:56:17 UTC) and 6 April (08:19:17 UTC) in 2019. This occurrence is not especially rare; ~900 new dated impacts have been discovered in the last decade on Mars using similar techniques (Daubar et al., 2013; Malin et al., 2006), although the imaging date constraints are usually on the order of a few years rather than a month. This impact was also extraordinary in its location very close to the recently landed InSight mission. At this distance, the prospect of detecting the impact event using the seismic and atmospheric instrumentation on InSight was an exciting possibility. This is the only impact we know to have formed this close to the lander during the time since InSight landed on Mars on 26 November 2018.

The new crater is located at 3.866°N planetocentric latitude, 135.613°E longitude, just 37.36 km from InSight, which landed at 4.502°N, 135.623°E (Parker et al., 2019). It is located along an azimuth of 180.9°, almost directly south of the lander. The asymmetric low-albedo blast zone pattern around the crater (Figure 1d), caused by the disturbance of light-toned dust during the impact, indicates a somewhat oblique impact coming from the southwest direction. Small dark spots to the southwest of the crater could be blast zones around secondary craters or multiple smaller primary craters in a clustered impact that formed when the impactor fragmented in the atmosphere (Daubar et al., 2019). Craters within these smaller dark spots are not resolved. The pattern of dark spots is more consistent with a clustered impact than with secondary craters; secondary craters would be concentrated downrange rather than uprange and typically have more symmetric radial patterns. In either case, the contribution of the group of smaller craters to a combined seismic signal would be negligible compared with that of the main ~1.5 m diameter crater (Schmerr et al., 2019).

A second HiRISE image was acquired to obtain stereo data, but the crater is not resolved in the resulting Digital Terrain Model (DTM). (See anaglyph in Figure S1 in the supporting information.) A depth of a few tens of centimeters is estimated for the new crater. Although this depth is not resolved in the DTM, an estimate was possible by scaling from larger, resolved, craters in the DTM.

In subsequent sections, we derive the expected seismic and atmospheric signals that would have been produced by this known impact and have the potential to have been detected by InSight (section 2). In section 3,

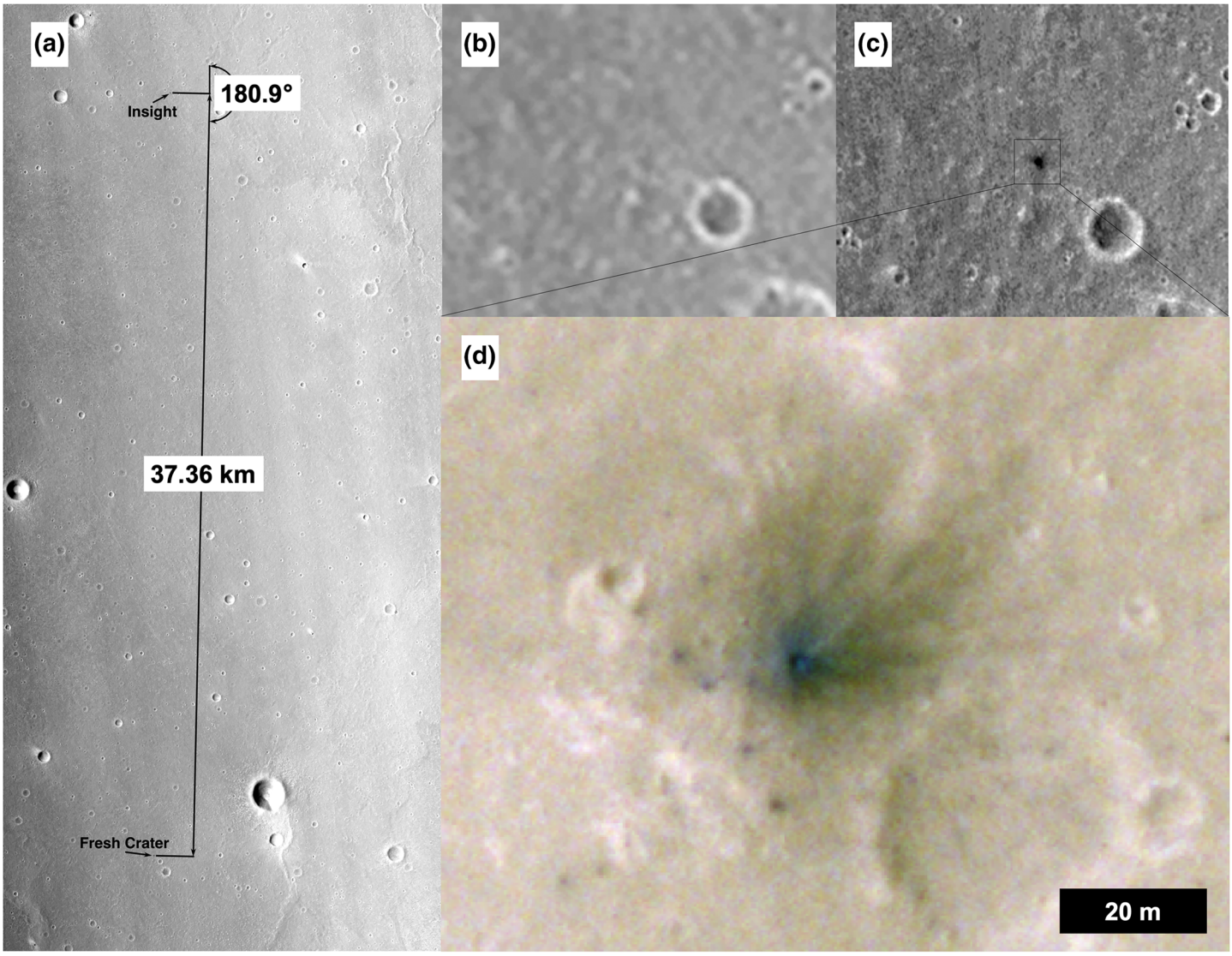

Figure 1. New crater observations. (a) CTX context image showing locations of InSight lander and new dated impact. (b) CTX image K14_068929_1845_XN_04N224W_190221 taken February 21, 2019 (6 m/px). (c) CTX image K16_059495_1829_XN_02N224W_190406 taken 6 April 2019, showing new dark spot that was not present in previous image. (d) Cutout from HiRISE image ESP_060128_1840 (COLOR RDR; 25 cm/px) showing new impact crater. North is up, and images have been stretched for contrast. Image credits: NASA/JPL/MSSS (CTX); NASA/JPL/University of Arizona (HiRISE).

we describe the search of the seismic data during the time period constrained by the before and after CTX images and the three candidate seismic events that were found. We then evaluate which of those seismic events and any associated atmospheric signals might be connected with the formation of the new crater. Finally, in section 4, we use InSight mission experience thus far to reevaluate the seismic impact discriminators we identified before landing, and we present updated expectations for impact detections with InSight in light of real data acquired since landing.

2. Predicted Signals From the New Impact Crater

2.1. Predicted Impact Parameters From the Observed Crater

To assess the detectability of the observed ~1.5 m diameter crater by InSight, we first estimate the impactor parameters. The geology of the impact target area is very similar to that in the immediate vicinity of the InSight lander, which has been characterized in detail (Golombek et al., 2020). The material in which the crater formed is likely to be a loose, porous regolith with very low cohesive strength ($\lesssim$50 kPa). The

diameter of meter-scale impact craters formed in such a material is expected to scale as a power of the vertical impactor momentum, with only minor additional dependence on other impactor parameters (Holsapple, 1993; Holsapple & Housen, 2007). For a 1.5 ± 0.25 m diameter crater, the predicted vertical impactor momentum is 100–3,000 Ns, depending on the cohesive strength of the regolith (Figure S2). The lower limit applies if the Martian regolith can be represented as cohesionless dry sand; a nominal upper limit applies if the Martian regolith has an effective cohesive strength of 50 kPa. An even higher impactor momentum is possible but that would require a cohesive strength of a well-cemented terrestrial soil, which is not compatible with observations of the Martian regolith made in the vicinity of the InSight lander (Golombek et al., 2020).

The seismic source of the impact can be expressed as an equivalent seismic moment, which scales approximately linearly with impactor momentum according to two independently derived, semiempirical scaling relationships (Gudkova et al., 2011, 2015; Shishkin, 2007; reviewed in Daubar et al., 2018). For an impactor momentum of 100–3,000 Ns, these relationships predict an equivalent seismic moment of 10^6–10^7 Nm (Figure S3).

The estimated impactor momentum implies an impactor mass ~0.1 to ~1 kg, depending on impact speed. Meteoroids in this mass range are substantially decelerated by Mars atmosphere (Figure S4) and are predicted to lose approximately 90% of their initial kinetic energy, 75% of their initial speed, and 30% of their initial mass by ablation and drag before striking the ground (Table S1). Thus, vertical impact speeds at the ground in the range of only 1–3 km/s are expected for typical preentry meteoroid encounter speeds of 5–15 km/s (JeongAhn & Malhotra, 2015; le Feuvre & Wieczorek, 2008) and entry angles of 15–90°. At these relatively slow impact speeds and taking into account the uncertainty in impactor momentum, estimates of the impact energy range from approximately 0.1 to 2 MJ (see supporting information Text S1).

An independent test of these energy estimates is provided by the empirical relationship from Teanby and Wookey (2011) between crater diameter (D) and impact energy (E), based on laboratory and field impact experiments, explosive analogs, and the Apollo artificial lunar impacts:

$$D = 8.8^{+2.6}_{-3.5} \times 10^{-3} E^{0.32 \pm 0.01} \left(\frac{g_\oplus}{g}\right)^{3/16}, \quad (1)$$

where $g_\oplus$ is Earths gravity (9.81 ms^{-2}) and g is Mars's gravity (3.73 ms^{-2}). The error bars incorporate scatter in the source data and the uncertainties in impact conditions. Using this relationship gives an estimated ground impact energy of 5.3 ± 1.8 MJ, which is somewhat larger than our previous estimate. We attribute this difference to the fact that most of the data used to construct Equation 1 are from experiments in terrestrial soils and rocks that have a much higher cohesive strength than the strength we adopt for the Martian regolith based on in situ and remote sensing of this region. Therefore, this scaling relationship provides an upper bound on the impact energy.

2.2. Predicted Seismic Signals Based on Energy and Moment Scaling

The estimated ground impact energy can be used to obtain a first order prediction of seismic P wave amplitude v at source-receiver distance x using scaling relations developed for terrestrial impacts (Teanby, 2015):

$$v(x, E) = a x^b E^c \quad (2)$$

where scaling law constants $a = 5.6 \times 10^{-5}$, $b = -1.6$, and $c = 0.5$ under Mars conditions (Teanby, 2015). The overall uncertainty on $v(x, E)$ is a factor of 4. This relationship is strictly only valid over the range of energies and distances used by Teanby (2015), which cover ~400–10,000 kg TNT equivalent (~2×10^3 to 4×10^4 MJ) (excluding the very high energy buried nuclear explosions) and 0.5–1,200 km ranges. These events had peak seismic frequencies in the range 1–16 Hz, with the Apollo lunar and Carancas Earth impacts peaking from 1 to 10 Hz. We can also estimate the longest timescale in the source function using crater excavation timescale, $\tau = \sqrt{(D/g)} \sim 0.6$ s, implying a frequency content of >1 Hz. Therefore, the scaling relationship is a reasonable, although not ideal, match to conditions for the new Martian crater, with the P wave frequency content likely peaking at a few hertz or slightly higher.

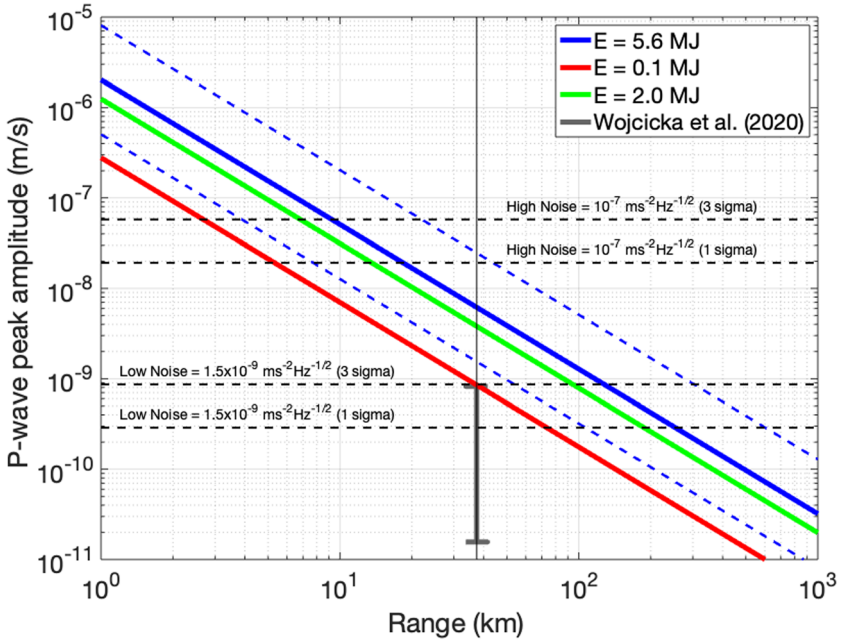

Figure 2. Estimated amplitude of *P* wave signal from the 1.5 m diameter new impact. The amplitude is estimated using the impact energy scaling relationship from Teanby (2015) in Equation 2 as described in the text. Solid lines show nominal amplitude prediction from scaling relations and uncertainty for three potential impact energies, a nominal range (red to green) and an upper limit (blue). Dashed blue lines show uncertainty on the upper limit E = 5.6 MJ case. Horizontal dashed lines show range of seismic noise measured at 4 Hz at the InSight landing site for 1σ and 3σ (Lognonné et al., 2019, 2020), and vertical black line shows the distance between InSight and the new crater. Gray vertical bar shows range of predictions from Wójcicka et al. (2020) from numerically derived impact momentum scaling. Seismic noise amplitudes are converted to equivalent velocities by integrating the amplitude spectral density noise for the 1–16 Hz bandwidth, using equation 14 in Teanby (2015). Amplitude estimates for the observed impact are at or below the noise levels.

A first order prediction of seismic *P* wave amplitude *v* for the new event is shown in Figure 2 compared to the range of measured InSight noise levels in the 1–16 Hz bandpass from Lognonné et al. (2019, 2020). The estimated *P* wave amplitude at the observed range of 37 km is 0.8–4 × 10^{-9} ms^{-1} for 0.1–2.0 MJ and 6 × 10^{-9} ms^{-1} with a factor of 4 uncertainty for the 5.6 MJ upper bound. Furthermore, Wójcicka et al. (2020) use numerical impact simulations to propose a recasting of the amplitude scaling in terms of impact momentum instead of energy, which relates to seismic moment more closely to linearly. When applied to impacts in relevant analog materials, this recasting results in a reduction in predicted seismic amplitudes by up to 2 orders of magnitude for small craters. Overall, these scaling laws have large uncertainties, and predictions span 3 orders of magnitude, but all imply a modest signal-to-noise ratio (SNR), with a likely SNR of only ~1 on average. These amplitude estimates are also in reasonable agreement with peak ground velocities predicted from numerical waveform simulations of the impact event (see supporting information Text S2). During the detection period, the continuous seismometer data coverage is limited to 10 sps (5 Hz Nyquist) sampling except during exceptional periods where 20 or 100 sps was collected (Figure S10). Therefore, any seismic energy over 5 Hz is unlikely to have been recorded for the majority of the time in question. The combination of low SNR, high frequency content, and low sample rate implies this event would have been be very difficult to detect seismically.

2.3. Predicted Seismic Signals Based on Lunar Impact Analogies

The closest seismic analog for this impact is the Lunar Module (LM) of Apollo 14, which impacted 67 km from the Apollo Lunar Surface Experiments Package station of Apollo 14. Its amplitude was about 40 data units on the vertical Long Period (LP) axis in peaked mode, corresponding to 2 nm of ground displacement at 2 s. See Lognonné et al. (2009) for a detailed analysis of this and other lunar impacts.

Table 1
Comparison Between the Source Parameters of the Apollo 14 Lunar Module (LM) Impact and the CTX Image-Constrained Impact That Formed the New 1.5 m Diameter Crater Discussed in This Paper

Impact	Distance from seismometer (km)	Velocity (km/s)	Angle (° from vertical)	Mass (kg)	Mv (Mv_z) (kg m/s)	Rim Diam (m)	Depth (m)	Formation time
LM Impact on the Moon	**67**	**1.68**	**86.4°**	**2,383**	4×10^6 (2.5×10^5)	6.5	1.37	0.94 s
New 1.5 m Crater on Mars	**37.4**	1–3	Not well constrained; moderately oblique	0.1–1	1.4×10^2 to 4.3×10^3 (1×10^2 to 3×10^3)	**1.5**	A few tens of centimeters	~0.30–0.35 s

Note. Parameters from the LM impacts are from Lognonné et al. (2009) and references therein. A 45° impact angle is assumed for the Martian impact, although this is only weakly constrained. Formation time is estimated from Holsapple (1993) and using $0.5\sqrt{(D/g)}$ as an estimate of the crater growth time (Schmidt & Housen, 1987). Known values are given in bold, and other values are inferred.

At such a small epicentral distance, intrinsic attenuation can be neglected, and the seismic signal is mostly constrained by the elastic propagation properties, which are mostly diffusive on the Moon, and the source parameters. These parameters are summarized in Table 1.

According to Sato and Korn (2007), the maximum amplitude of a pulse propagating in the multiple forward scattering regime is proportional to $\sqrt{\frac{1}{xT_m}}$, where x is the hypocentral distance and T_m is a characteristic time scale. T_m depends on the heterogeneity of the medium as follows:

$$T_m = \sqrt{\pi} \frac{< \varepsilon^2 > D^2}{2\alpha\beta} \tag{3}$$

where β is the wave propagation speed, α is the correlation length of the random fluctuations, and their variance is $< \varepsilon^2 >$. This theory predicts that the typical maximum amplitude is proportional to $\sqrt{\frac{\alpha\beta}{x^3 < \varepsilon^2 >}}$. Note that these formulae are valid in media with velocity and density with gaussian fluctuations (Sato & Korn, 2007).

We do not expect the correlation distance to differ significantly between Mars and the Moon, but fluctuations are certainly stronger on the Moon because scattering is stronger. As the diffusivity is inversely proportional to $< \varepsilon^2 >$, we expect the amplitude to be 5 to 10 times larger on Mars than on the Moon, for the same source and distance, following initial comparisons of the crustal diffusivity (Lognonné et al., 2020).

With these assumptions, we can convert amplitudes of impacts detected on the Moon to the Martian situation. Following previous work (Gudkova et al., 2011, 2015; Lognonné et al., 2009), we assume that the amplitude of the signal is linearly related to the vertical momentum, which implies a source for the Martian impact smaller in moment than the LM source by a factor of ~83–2,500. On the other hand, the difference in diffusion makes the maximum amplitude of the signal larger by a factor 5–10. Last but not least, the difference in distance for the LM impact at 67 km makes the signal larger by a factor of 2.37 for an −1.5 exponential decay, comparable to the −1.6 power law decay of local magnitudes on Earth at short distance (Richter, 1958). Combining these factors, this suggests a Martian signal smaller than the lunar one by a factor of 8.3–500 without a geometrical spreading correction; with that correction, it would be smaller by a factor of 3.5–210.

The duration of the signal can also be addressed with similar analogies. Martian signals are expected to have much shorter durations than lunar ones due to the ratio of diffusivities. Rise times are found to be in the range of 600–800 s for lunar impacts (Gillet et al., 2017) and are expected to be reduced by a factor of 30–100 for Mars. Signals with SNR of 3 will have durations of about 2–3 times the rise time, leading to durations in the range of 20–60 s for each phase in this case.

In summary, based on early estimates of the diffusivity of Mars, we expect this impact on Mars to have a signal smaller in amplitude by a factor of 3.5 to 210 compared to the Apollo 14 LM impact recorded by the Apollo 12 vertical LP instrument. Martian impact signals are also expected to have much shorter durations of ~20–60 s.

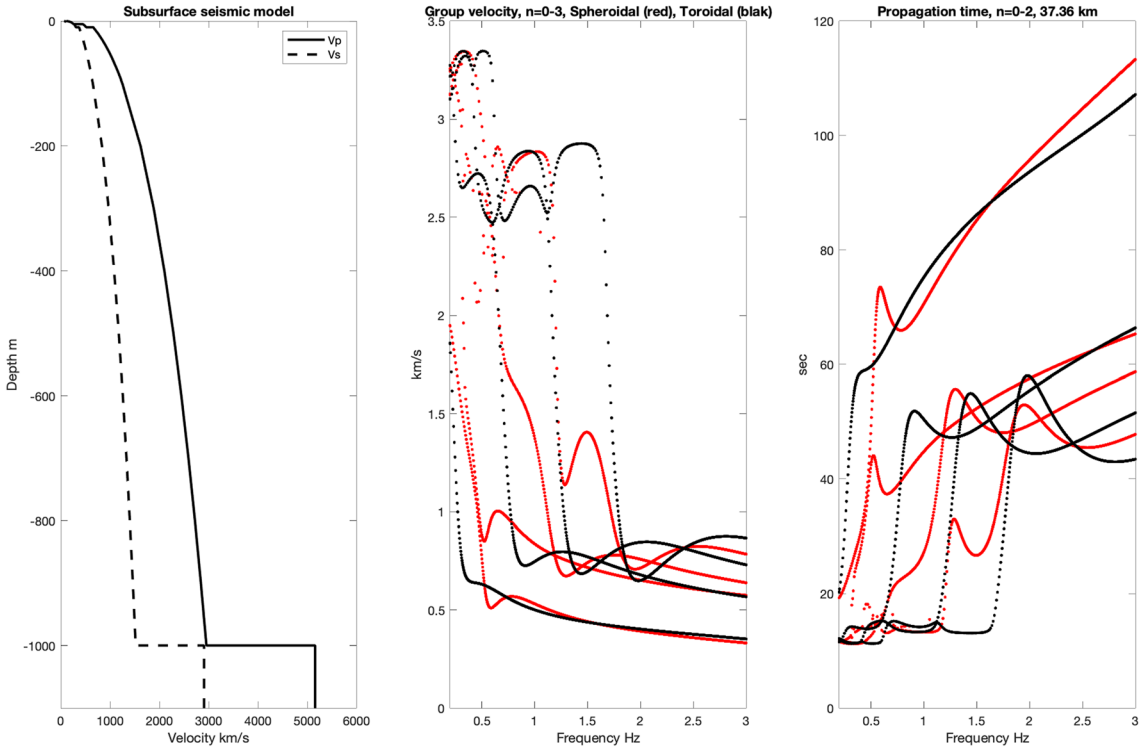

Figure 3. (left) Subsurface seismic model. (middle) Group velocities of the fundamental Rayleigh and Love waves and of the three first spheroidal (red) and toroidal (black) overtones. (right) Propagation time of the surface wave packet to a distance of 37.36 km, as a function of frequency up to 3 Hz. Model data is provided in Table S2.

In order to estimate propagation time differences between the main phases, we use the fact that an event at a distance of 37 km in a homogenous Martian crust will propagate down to a depth of ~500 m. We can expect that most of the energy of this event will therefore be guided in the first half kilometer of depth, for which seismic velocities are expected up to 2,000 m/s for *P* waves and 1,000 m/s for *S* waves. Most of the energy will be in surface waves, for which typical group velocities are computed with Mineos software (https://geodynamics.org/cig/software/mineos/) (Figure 3a). These are shown for one possible model of the shallow subsurface structure based on constraints proposed by Lognonné et al. (2020) for the first 5 m of depth, measurements of the seismic velocities of layers of volcanic material (Lesage et al., 2018) down to 1 km depth, and the TAYAK reference model below that (Smrekar et al., 2019). See supporting information Text S3 for details of the model. Note that apart from the first 5 m, this model is merely representative, constrained only by earth analog. Propagation times (Figure 3b) range from 11–15 s to 80 s for the four first spheroidal/toroidal surface wave branches. We note that the ratio between the fundamental and the harmonic group velocities can be much larger than the standard $\sqrt{3}$ ratio between the velocities of *P* and *S* body waves used by Marsquake Service (MQS) (see section 3). As an example, the 78 s between the two phases of event S0116a (discussed in section 3.1) are compatible with a slow packet propagating at 360 m/s (roughly the shear wave velocity at the base of the bedrock in our model) and a second packet propagating four times faster, which is roughly the *P* wave velocity at a depth of ~100 m, as proposed by Lesage et al. (2018). A difference of several minutes between the arrival of the first and second pulse is also found in event S0105a (see section 3.1). Second arrivals such as these might also be fundamental scattered Rayleigh waves, while the first arrivals could be overtones propagating in the deeper bedrock. The group velocity of the subsurface models also shows a clear variation of the group velocity just above 0.5 Hz, which might be the reason the signal has a cutoff frequency ~0.5 Hz.

In summary, based on lunar data extrapolated to Mars, the shallow layers and diffusivity of Mars suggest that for an event at the distance of the new crater, we expect phase durations of 30 s to 1 min, with differences in phase arrivals up to about 1 min.

2.4. Predicted Atmospheric Signals

A meteor entering the atmosphere and causing an impact crater would generate at various atmospheric levels in the entry path and at impact time both low-frequency gravity waves (typically 0.01–0.001 Hz) and high-frequency acoustic waves (frequencies above 0.01 Hz, typically 1–100 Hz) (Garcia et al., 2017; Karakostas et al., 2018; Revelle, 1976; Spiga et al., 2018). Those signals could be detected by a high-sensitivity pressure sensor operating continuously such as the pressure sensor in the Auxiliary Payload Sensor Suite on board InSight (Daubar et al., 2018).

An airburst signal would be characterized by two arrivals: first, the main seismic signal of surface waves excited at the location of the impact and, second, the blast wave through the atmosphere exciting the ground at the lander (Stevanović et al., 2017). A differential travel time of ~2 min is expected between two such signals due to the difference in wave propagation speeds of 230 m/s in the air and 1.5 km/s in the subsurface over the 37 km distance from the impact to the lander. Such a signal would be much smaller than InSight's pressure sensor limit of detectability, so SEIS would be the only way to detect such a phenomenon.

Atmospheric entry modeling demonstrates that for this scale of impact the majority of the meteoroid's kinetic energy is transferred to the atmosphere during deceleration and ablation, and only a small fraction is directly coupled to the ground by the surviving fragment(s). The relatively large blast zone surrounding the crater (Figure 1d) is testament to this partitioning. However, previous work suggests that detection of the direct ground impact is more likely than detection of airburst-generated acoustic and gravity waves near the ground surface (Garcia et al., 2017) as InSight's detection capability of acoustic and gravity waves produced by airbursts and surface explosions is negatively affected by atmospheric attenuation and propagation conditions less favorable than on Earth (Lognonné et al., 2016). Moreover, numerical modeling (based on the methodology of Karakostas et al., 2018) suggests that even in the end-member case of all the meteoroid kinetic energy being deposited in the atmosphere, the resulting air-coupled seismic waves would still not be detectable by the InSight instruments. Acoustic ray propagation models (Garcia et al., 2017; Spiga et al., 2018) show the trajectories of infrasound rays do not reach the InSight lander, which is in an unfortunate shadow zone at this distance from the impact (Figure S11). Considering both atmospheric wave propagation conditions and meteor energy scaling, we therefore do not expect the acoustic and gravity waves generated by the meteoroid that formed the 1.5 m crater to be detected by InSight.

3. Candidate Seismic Events in the Time Period of Interest

3.1. Description of SEIS Data and the Candidate Events

The time between the before and after CTX images was a period of immense interest in the data coming from InSight. The most relevant data was from the seismometer, Seismic Experiment for Interior Structure (SEIS; Lognonné et al., 2019). This temporal search window occurred as SEIS commissioning was being finalized, only a few weeks after SEIS was placed on the ground (17 January 2019) and the Wind and Thermal Shield had been placed over it (2 February 2019), allowing the lowest possible noise on the instrument. Fortunately, continuous data collection (InSight Mars SEIS data Service, 2019) had already transitioned to being round the clock and three-component very broadband (VBB) and short period (SP) data at 10 sps, sometimes also at 20 sps, was available throughout the time period (Figure S10).

Figure 4 provides an overview of the completeness, the noise, and the occurrence of seismic signals in the data within the search window. Seismic noise on Mars clearly falls into a daily pattern, with low noise only occurring between ~16:00 LMST (local mean solar time) to ~02:00 LMST (Giardini et al., 2020; Lognonné et al., 2020). Outside of this time, there is a substantial increase in noise, with steady winds in the early morning followed by a gusty midday period. During these times, only very strong seismic signals can be detected. Furthermore, not all days include a significant quiet period. Thus, there are large daily and day-to-day variations in our capacity to detect weak seismic events on Mars using SEIS data. During the search window, we estimate weak signals could be reliably detected only ~30% of the time.

Despite these limitations to the data, three potential seismic events were identified between the times of the constraining CTX images (Figure 4). Although all three are weak signals, there are unique aspects of these events that deserve examination. We discuss the characteristics of each of them and the likelihood that each is the signal resulting from the observed new crater.

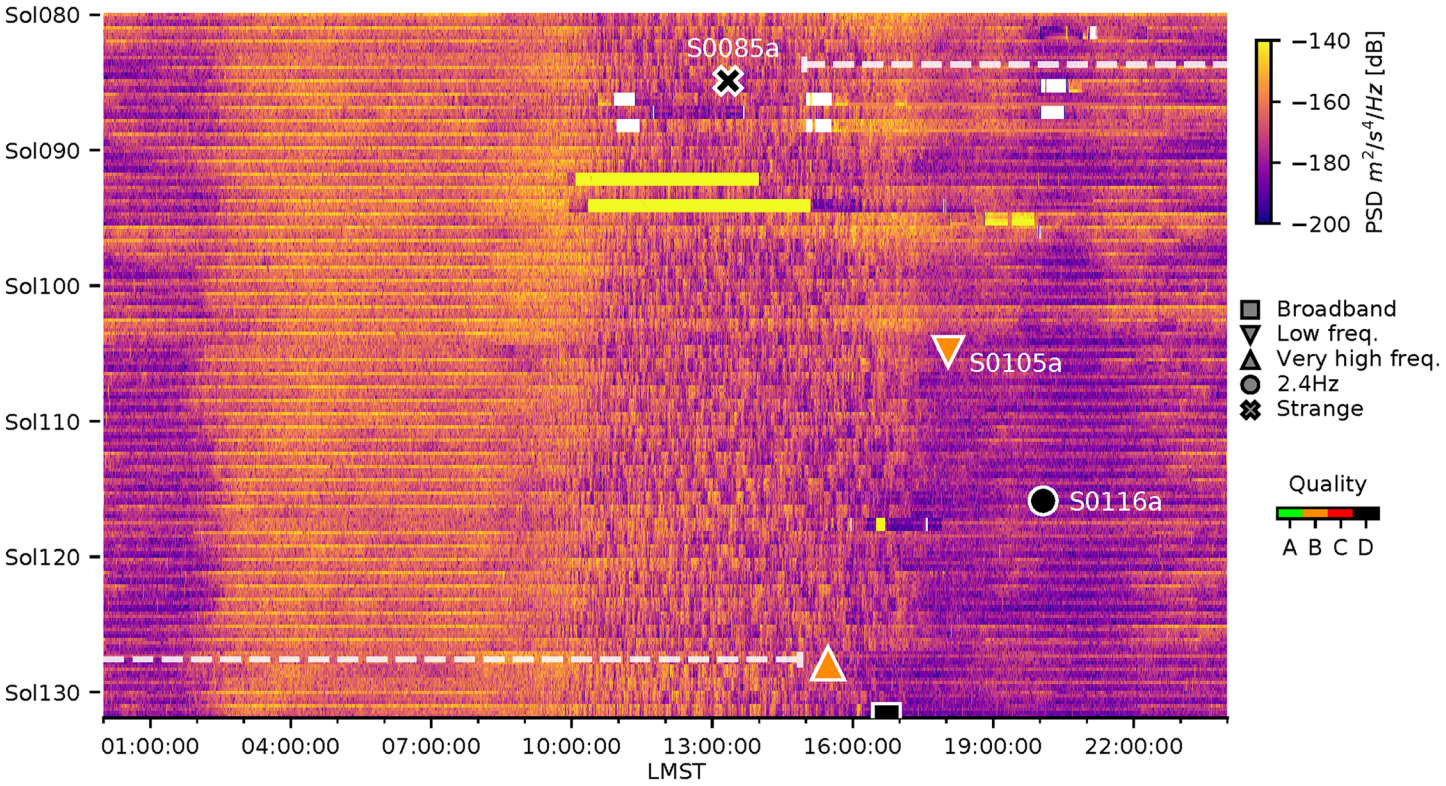

Figure 4. Spectrogram stack from InSight sol 80 (16 February 2019) to sol 132 (10 April 2019). This period bounds the impact search window from sol 84 14:55 LMST (21 February 2019 03:56 UTC) to sol 127 14:18 LMST (6 April 2019 08:20 UTC), indicated by start/end of the white dashed lines. Each horizontal line in this plot corresponds to a sol-long acceleration spectrogram from 20 s to 4 Hz for the vertical VBB component. White and yellow bars indicate data gaps and amplitude saturation, respectively, occurring during sensor calibration and hammering of the heat flow probe. The three events detected and discussed in this paper are marked with symbols corresponding to the event type, while event quality is indicated by symbol color (see legend). Two events that occurred just after the end of the search window are also indicated.

The MQS (Clinton et al., 2018) is tasked with reviewing all data from SEIS, detecting and characterizing seismic energy, and maintaining a catalogue of marsquakes. MQS detects events by careful manual review of all continuous data. Over the course of the mission so far, the most effective approach to identifying marsquakes has proven to be data review using spectrograms. Standard MQS operations produce daily spectrograms with a window length of 50 s for frequencies below 1 Hz and 10 s for higher frequencies. In the first months, two major event families have been observed (Giardini et al., 2020; InSight Marsquake Service, 2020). The first family is characterized by events with energy dominant at lower frequencies, visible as a 10–20 min long energy surplus between 0.1 and 3 Hz. This family comprises the two event types, low frequency (LF) and broadband. The largest of these events (named S0173a and S0235b; Giardini et al., 2020, Lognonné et al., 2020) have clearly identifiable *P* and *S* waves, with clear polarization showing the direction as seen from the lander, followed by long codas of scattered energy. Smaller events of this type have polarities that are less clear or are not detectable, but the envelope of the waveforms and their spectral content supports the interpretation that they are smaller versions of the same type of event. The second major family includes high frequency (HF) events, characterized by an energy content mainly above 1 Hz, an extended coda, and a lack of polarization. An additional curious feature of the InSight landing site is a local seismic resonance at 2.4 Hz. For larger HF events, the spectrum can be matched by a general earthquake spectrum, taking into account source size and attenuation, modulated by an amplification of 12 dB in spectral energy around 2.4 Hz. For smaller HF events, only this peak is visible, while the bulk of the energy is below the ambient noise level. Events in this family are classified as high frequency, very high frequency, or 2.4 Hz. A handful of events have been documented as "strange" if they do not fit into any of these standard event types.

During the time period of the impact search, one event was found during standard MQS operations. It has the label S0105a (the first seismic event to occur on sol 105 of the mission) and is a low frequency event.

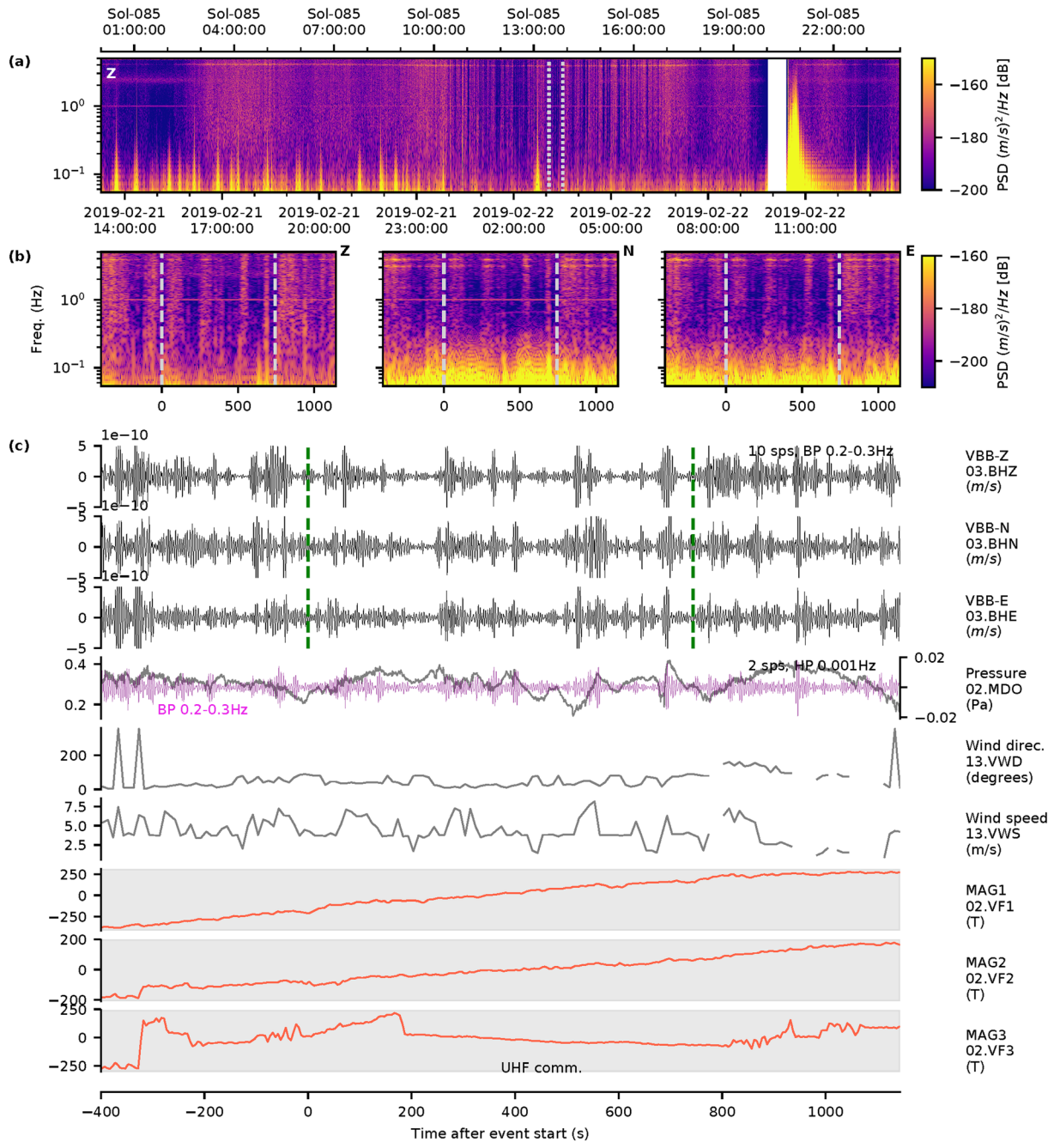

Figure 5. Summary of S0085a event. (a) The context of the event in the full sol spectrogram on the VBB vertical (Z) component. (b) Spectrograms for all three VBB components rotated into Z, north (N), and east (E) orientations. The start and end time are indicted by the vertical dashed white lines in (a) and (b). (c) Time series from the three VBB velocity, pressure, wind direction, wind speed, and three magnetometer channels. The data are filtered as indicated to accentuate seismic and pressure signals. The vertical green dotted lines in (c) indicate the event start and end times. In general, in these summary figures, additional phase picks in green and glitch windows in red are overlain on the seismic channels and on the magnetometer channel indications of any reported lander activity are shown in gray. For this event, however, the lander has UHF communications, there are no major glitches, and the event is too weak for MQS to identify phases. This event is extremely faint and not visible in the time series. The event is the very narrow band of energy at 0.7 Hz visible on the N component spectrogram. As explained in the text, this signal may not have a seismic source.

It was in fact the first seismic event detected during the whole mission. After the CTX discovery of the impact, a review of all data during this period was performed by the InSight team, both within and independently of the MQS team. This review took into account the improved understanding of marsquake character that had accumulated from other events in the meantime. During this review, two

additional events in the time period were identified: a small high frequency event on sol 116 and one unclassifiable seismic signal on sol 85. We first describe the three events in detail:

A summary of the S0085a event is shown in Figure 5. This event, which appears to be unique among events detected on InSight thus far, consists of a very narrow-banded energy surplus at 0.7 Hz, with a bandwidth of 0.05 Hz. There is a slight rise in frequency over the course of the event, from 0.57 Hz up to 0.7 Hz. The signal is visible dominantly on the north component, with weak traces in the Z (vertical) component. This indicates a clear N/S azimuth. The signal occurs only hours after the opening of the search window, during the part of the day with high atmospheric noise. In fact, it is interrupted by several wind bursts creating noise more than 10 dB above the signal itself. Because it can only be resolved during the intermittent quiet periods, the exact start and end times cannot be positively identified, but the event lasts at least 10 min. The very narrow bandwidth does not fit any expected seismic mechanism (including impacts). A similar signal has not been observed a second time during the mission, especially not during a quieter period, which would allow a better classification of its character. No particular lander activity was going on at the time of this event that could explain it. Given the high atmospheric noise surrounding this time, it cannot be discounted that it could be of random origin.

This event was not detected using standard analysis, but extending a method that exploits the ratios of the average energy residing 2.4 Hz $\pm$ 0.2 Hz, to different frequency bands of the SP's and VBB's north, east, and vertical (Z) components. The algorithm was implemented in steps of 0.4 Hz with 50% overlapping windows in frequency and avoiding injection of tick noise (cross-talk noise generated by the SEIS temperature signal on the VBB and SP seismic data). The resulting outliers were inspected against the average energy in the energy short-term average channel (defined as the root-mean-square of data filtered within a 0.5 s time window; Lognonné et al., 2019), to ensure they occurred during calmer atmospheric periods and to allow for further investigation.

S0105a (2019/03/14 21:03:31, 18:07 LMST; MQS classification: low frequency, Quality C).This low frequency event consists of two energy pulses, each without clear polarization (Figure 6). It occurs around sunset, just after the transition from the high atmospheric situation of the day into the very quiet early evening. The amplitude of this event is so low that it could only have been reliably detected during ~25% of the time period of the impact. The total length of the signal is ~15 min, with at least 5 min uncertainty, given the relatively high noise level. The spectral energy is above the ambient noise between 0.3 and 0.5 Hz for the first pulse and 0.15 and 0.5 Hz for the second pulse. The spectrum of the two pulses is comparable to that of event S0173a, currently the largest LF event in the MQS catalogue but 16 dB lower at 0.3 Hz. The phases are emergent, and phase arrival picks for the two energy pulses cannot be made in the time domain and so are made using a spectrogram and accordingly assigned high uncertainties of $\pm$20 s. In the time domain, the separation of the two pulses is also similar to that of S0173a (160 s for S0105a vs. 155 s for S0173a). The similarity of the signal of this event and other low frequency events is shown in Figure 3 from Giardini et al. (2020) and consistent with other larger events of this type, we assign *P* and *S* phases to the onset of these pulses. It would be difficult to convincingly assign these phase arrivals to *P* and *S* waves without the context of the wider seismicity so far recorded by InSight. Other interpretations may also be plausible, as discussed above in section 2.3, though this weak event is generally similar to stronger and more well-understood events.

Based on the time elapsed between these pulses, this event is estimated to be located at a distance of 27 $\pm$ 5° (1,600 $\pm$ 300 km). For S0173a, a polarization analysis was also possible, resulting in a direction of the events as seen from the lander of 91 $\pm$ 5°; thus, it has been concluded this is the signal of a marsquake located in the Cerberus Fossae graben system (Giardini et al., 2020). This fault system is the only place on Mars where more than one marsquake has been located so far, in agreement with premission hypotheses of seismic activity there. A possible interpretation of the S0105a event is therefore that it is a smaller tectonic marsquake in a similar location to S0173a. As no polarization could be determined for S0105a, this interpretation must remain preliminary. The low signal-to-noise ratio also implies that no depth could be estimated for this or any other event in the impact time period.

S0116a (2019/03/26 06:27:19 UTC, 20:11 LMST; MQS classification: High Frequency 2.4 Hz, Quality D). This high frequency 2.4 Hz event, summarized in Figure 7, consists of an energy surplus around the 2.4 Hz mode of about 7 dB in displacement power, concentrated into two pulses separated by 78 $\pm$ 10 s. At the time of detection, this event was unique, but as of the time of writing, we have come to realize that it was just the

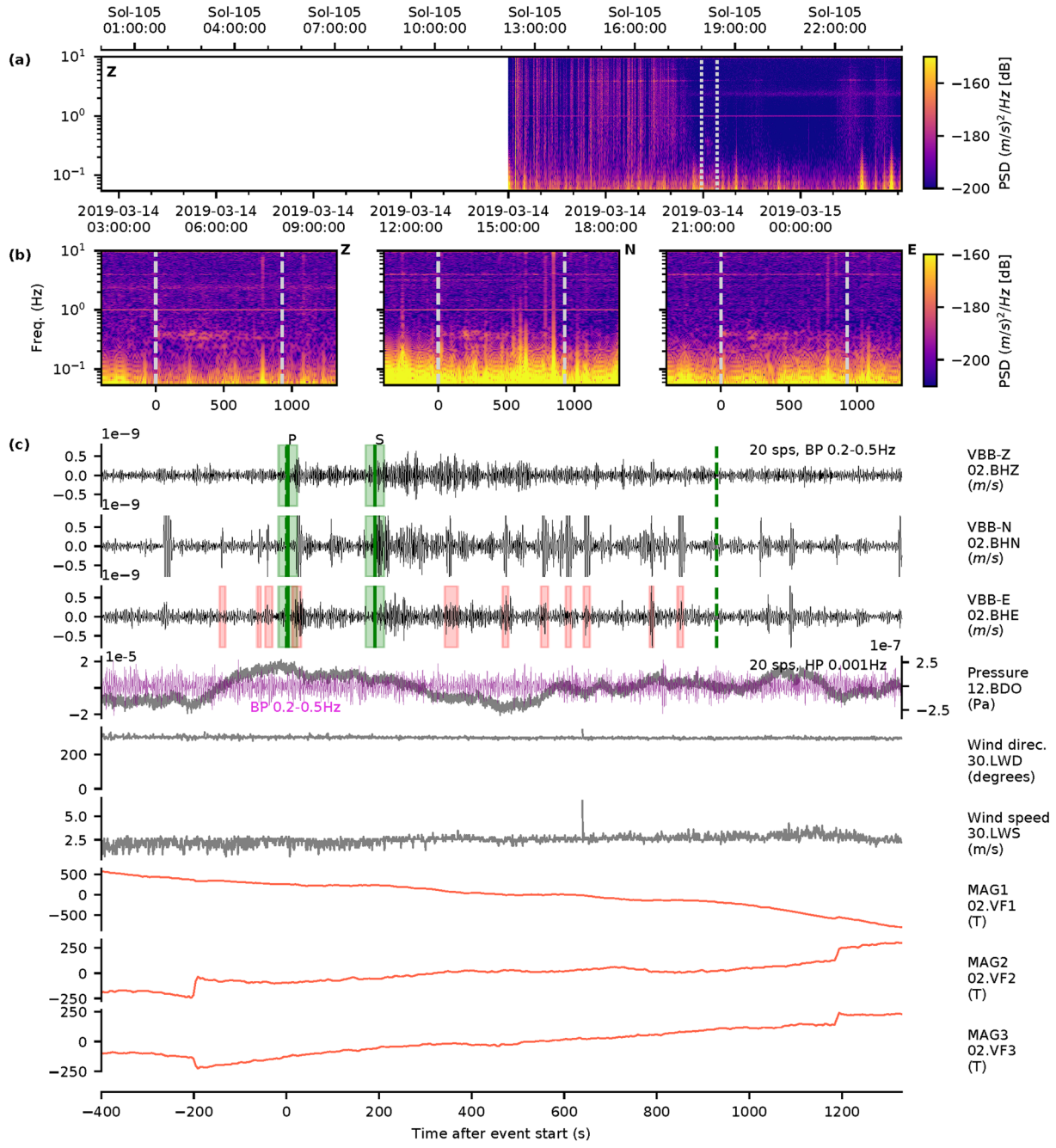

Figure 6. Summary of S0105a event, following Figure 5. During this event, there are multiple glitches (red shaded windows), most clearly visible in the E component, and no lander activity. MQS also identifies *P* and *S* phases (green solid vertical lines). Event energy is visible on all three components in both time series and spectrograms.

first occurrence of a general class of similar events, termed "2.4 Hz events." These are currently understood as being small high frequency events. HF events are interpreted as shallow-source events occurring in a highly scattering layer in the upper crust, probably shallower than the source region of the LF events. The absolute distance of the HF events cannot be determined yet, as crustal seismic velocities are so far unknown. The convention for these HF events is to label the start of each pulse as Pg and Sg phases. From the separation of the two phases, a relative distance can be estimated. The S0116a event is about four times closer than the majority of the HF events occurring later in the mission, so it seems to have

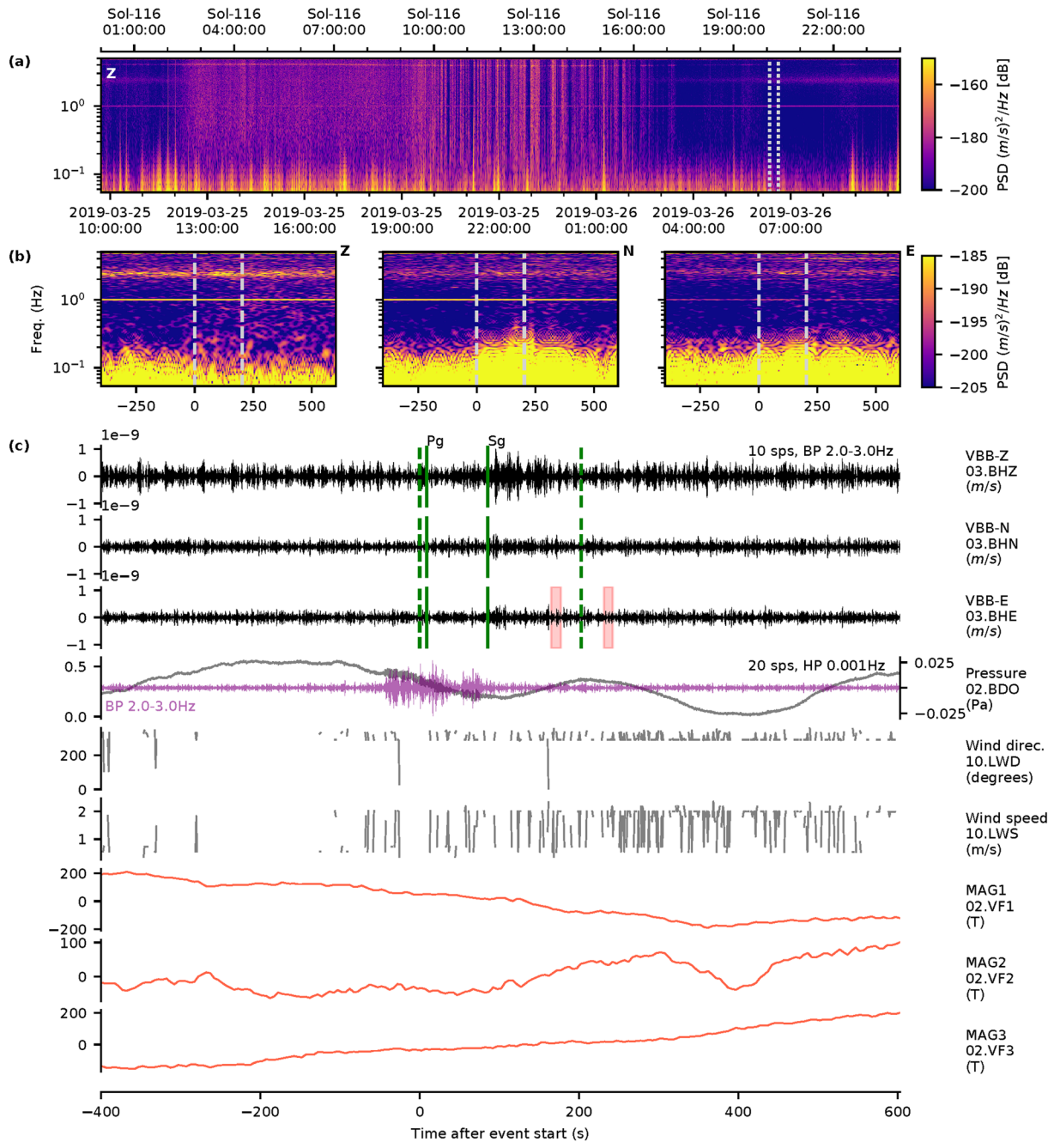

Figure 7. Summary of S0116a event, following Figure 5. During this event, there are two minor glitches toward the end of the event (red shaded windows), and no lander activity. MQS also identifies tentative Pg and Sg phases (green vertical bars). Event energy at the 2.4 Hz resonance is weakly visible on all three components in both time series and spectrograms. An anomalous high frequency disturbance in the 2 sps pressure precedes the event, extending into the first minutes.

emanated from a difference source region. Only a handful of other events share a similarly short Sg-Pg interval. Nevertheless, for it to have occurred at the detected impact site, the shear wave velocity in the medium would have to be as low as 210 m/s (assuming a v_P/v_s ratio of $\sqrt{3}$). Such a velocity is found in bedrock layers 5–10 m deep (Lognonné et al., 2020) but is unlikely at these shallow depths. In the MQS catalogue, all HF events are given an estimated location using an assumed S wave velocity of $v_s = 2.3$ km/s and P wave velocity of $v_P = \sqrt{3}v_s = 4.0$ km/s. Using those assumed velocities, this event has an

Table 2
Expected Characteristics of the Seismic Signal Produced by the Known Impact, Compared to the Characteristics of Each of the Candidate Seismic Events

	Unambiguous Seismic event?	Amplitude (nm/s)	Peak frequency (Hz)	Polarization	Duration (min)	Distance to source (km)
Predicted for known impact:	*Uncertain*	*~0.8–4 nm/s*	*~2–3 Hz most likely for body waves*	*180.9° (approximately N/S)*	*30 s–1 min*	*37.4 km (0.65°)*
S0085a	No, very unusual signal occurring in noisiest time period ~	0.3 nm/s (North; Vertical and East not above noise) (bandpass 0.5–1 Hz, 6 pole) (approximately right) ✓	0.7 Hz (too low) ✗	N/S ✓	~10 min Too long ✗	Unknown ~
S0105a	Yes, clear LF event ~	1.5 nm/s (East), 0.5 nm/s (Vertical; North affected by glitches) (bandpass 0.2–0.67 Hz, 6 pole) (approximately right) ✓	0.15–0.5 Hz (too low) ✗	None identifiable ~	~15 min Too long ✗	1,600 ± 300 km (27 ± 5°) ✗
S0116a	No,weak 2.4 Hz resonance ~	0.7 nm/s (Vertical) 0.5 nm/s (East) 0.5 nm/s (North) (bandpass 2.2–2.8 Hz, 6 pole) (approximately right) ✓	2.4 Hz (reasonable) ✓	None identifiable ~	~3 mins Too long ✗	Unknown ~

Note. Matching characteristics are marked with a green check mark, nonmatching characteristics are marked with a red "X," and neutral or undetected characteristics are marked with a black "~". Distance to source is measured from orbital images for the known impact and estimated for seismic events by MQS.

estimated distance of 11°, ~640 km from the InSight lander. As the event is only visible as an excitation of the 2.4 Hz mode, its original source spectrum cannot be constrained.

The amplitude of this event is so low that it could have been detected during only ~20% of the day during the time period of the known impact.

We note that nearly exactly 1 sol after the search period closed, the very high frequency event S0128a occurred. It can be seen in Figure 4 but outside the search period defined by the dashed white lines. This was one of the largest events so far recorded and one of the events located closest to the InSight lander, although it is still estimated to be roughly ~8° ± 6° (~480 km ± 350 km) away (Giardini et al., 2020; Lognonné et al., 2020). Although the uncertainties on this distance estimate are large, they still do not encompass the small distance to this known impact. Additionally, the timing of the CTX images has been closely compared to this event timing, and the event does not fall within the possible time period for the new impact.

3.2. Evaluating Seismic Data for the Candidate Events

With regard to the three events detected within the search period, how can we evaluate which, if any, is the recording of the known image-constrained impact? Aside from their occurrence within the search period between 21 February 2019 and 6 April 19, there are few other positive indicators that each of the signals was caused by the impact. Scaling relationships and analog comparisons predict the observed impact would create a seismic signal with peak energy approximately a few hertz, with a peak amplitude of the *P* wave ~0.8–4 nm/s. This range is also in good agreement with amplitudes from the numerical wave propagation simulations (supporting information Text S2). However, none of the three candidate events includes energy above 2.4 Hz. The predicted duration of the event is ~30 s to 1 min, although this is difficult to compare directly due to scattering. However, all candidate events have durations of over several minutes. We know the impact occurred at a back azimuth of 180.9°, so any polarization present in the signal should be in the north-south direction. S0105a and S0116a have no indication of polarization, though S0085a does include energy only in the N-S component, which is a match. Here we detail how well each of the candidate signals matches these expected characteristics (Table 2).

S0085a. The event on sol 85 is the only one of the candidates with a measurable polarization, and it is in the correct direction relative to the impact. However, it is possible that this event may not be a seismic event at

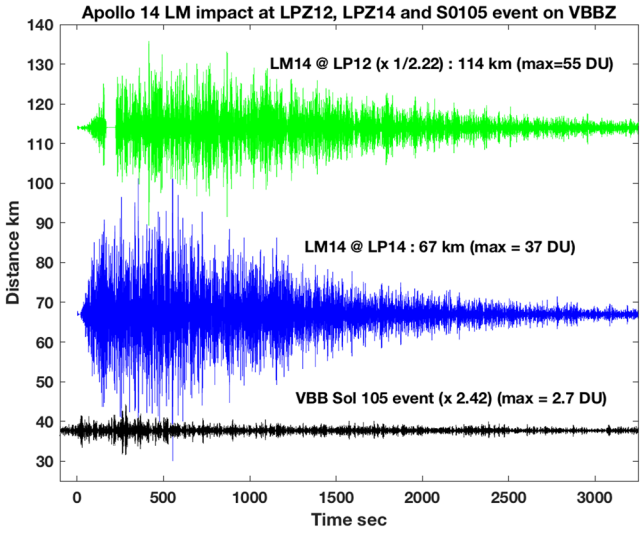

Figure 8. Comparison between the Martian event S0105a (black) and the Apollo 14 LM impact as recorded at two Apollo stations (green for Apollo 12 and blue for Apollo 14). The S0105a event has been deglitched (Lognonné et al., 2020) and converted into Apollo data units (DUs) by using the Apollo transfer function of the LP instruments. All events have been filtered with a sixth-order Butterworth bandpass between 0.2 and 0.67 Hz and corrected for the different distances by using a −1.5 power law with distance. Amplitude in DU as well as geometrical correction values are given on the figure. The very impulsive first arrival identified by MQS for S0105a is at time 0, followed by a second arrival 160 s later.

all—it could in fact be instrument-generated rather than a natural external source. Many spacecraft-induced signals will have a similar N/S polarization, as the InSight lander is toward the north of SEIS. Compared to other observed events, it has very narrow-band energy with an apparent dispersion, which is not expected for an impact. Even if this were a true seismic event, we cannot definitively identify it with the impact.

S0105a. The event on sol 105, on the other hand, is a clear seismic event. Its amplitude (0.5 nm/s in the 0.2–0.67 Hz bandwidth on Vertical and 1.5 nm/s on East) is at the lower end of that predicted. The spectral peak is at a frequency lower than that predicted. If this is an impact at ~40 km, it would have to be explained why tens of other seismic events detected so far look very similar to this one. It is exceedingly unlikely that multiple small impacts occurred in this region in the same time period and we do not have any images of them, although we do not have complete repeat image coverage of the region out to ~40 km away from InSight in order to rule this out completely. Without definitive criteria for discriminating between impact and tectonic sources (see section 4.1), we cannot exclude the possibility that one of these similar events is also an impact.

Figure 8 compares the S0105a signal with two Apollo impact records. All signals have been filtered with a sixth-order Butterworth bandpass (0.2–0.67 Hz), and SEIS data are expressed in Apollo digital units. Amplitudes in Figure 8 have been corrected with respect to distance using a −1.5 power law dependency with respect to the Apollo 14 LM impact recorded by the Apollo 14 LP seismometer, while the noncorrected amplitudes are given for each trace. The amplitude of the S0105 event is approximately 15 times smaller than that of the lunar LM impacts, which is within our estimate of a factor of 3.5–210 (see section 2.3). The amplitude of the signal at 0.5 Hz can therefore be explained by the size of the known impact. However, neither the lack of high frequencies nor the duration of this event is compatible with what we expect for this impact.

S0116a. The event on sol 116 has an amplitude at the lower end of that predicted, though this is on top of the 2.4 Hz resonance, so is likely amplified. It has a higher frequency than the other events, which is reasonable for a small, local event. No polarization was detected, so no direction or distance can be estimated. In the months since this event was recognized, hundreds of other similar events have occurred, again making it unlikely this is due to an impact, which would occur relatively infrequently.

In summary, none of the three events can be unambiguously identified as the seismic signature of the new impact. The S0105a event can be explained as a relatively small tectonic marsquake in the Cerberus Fossae region. The S0116a could possibly be caused by the impact, but given its low amplitude, it cannot be further classified or analyzed. Both S0105a and S0116a are similar to numerous other events in the marsquake catalogue, suggesting they are not produced by a local impact signal, which we expect to be a rare occurrence. The S0085a signal is extremely weak, and its very narrow-band nature suggests that it is not likely to have been caused by an external seismic event.

We note the extreme variation in diurnal noise means that significantly larger events than the three identified here may be hidden in the data. As noted, the amplitude we predict for this impact is quite close to the measured noise levels of SEIS during the least noisy time periods (Figure 4). Given daily and seasonal variations in temperature and wind activity, the noise levels are lowest in the evening (Lognonné et al., 2020; Figure 4). Signals on the order of the predicted amplitude would only be observable (at ~3 SNR) for ~20–30% of the time. Thus, the actual signal from this impact could very likely have occurred at a time when noise swamped the signal.

Another observational bias could occur due to the 2.4 Hz signals. These are a resonance seen in numerous other events (Giardini et al., 2020), and this is also near the peak frequency expected for impact event. Such a resonance could enhance smaller signals, allowing detection of signals that are otherwise approximately 10

times smaller if they are near the resonance. This might help our detection likelihood, but it is also a narrow band, making source discrimination more difficult.

3.3. Evaluating Atmospheric Data for the Candidate Events

Although no obvious atmospheric signals were associated with the three seismic candidates, each event was investigated to eliminate that possibility:

S0085a occurred in the local early afternoon (unlike the S0105a and S0116a events). Atmospheric variability for S0085a is thus mostly governed by convective turbulence (cells and vortices), usually found in daytime hours. There were no vortex signals close to the event that might have affected the seismic signal. Under normal conditions, gravity waves are not usually detected in daytime hours, based on the first 300 sols of InSight measurements (Banfield et al., 2020), and no gravity waves were detected around the time of this event.

There was no notable atmospheric signal associated directly with the S0105a event. Pressure and temperature measurements were uneventful, and the wind was steady and low. Two hours after the seismic event, a gravity wave of strong amplitude ($\pm$0.5 Pa) with a period of 400–600 s was detected. However, between sols 100–150, similar signals were very frequently seen at these local times (~20:00 LMST). Furthermore, given the proximity of the impact to InSight, a propagation speed that would cause a 2 hr delay between the seismic signal and the atmospheric wave packet is far too low to be realistic. This is based on typical gravity wave phase speeds estimated by Banfield et al. (2020) of ~20–30 m/s. The gravity wave signal reached InSight 2 hr after the seismic event; even accounting for background wind, the gravity wave would be too fast to have been emitted by the atmospheric entry of a meteoroid at 37.4 km distance. It is thus not likely to be related to the seismic event.

For S0116a, a gravity wave signal was found in the pressure signal at a time near the seismic event. However, it started about a quarter of an hour before the seismic signal, which implies the two are unrelated. Wind and temperature measurements behaved as usual for evening conditions at the InSight landing site. Interestingly, around the start of the event, just before the seismic signal, the pressure signal also underwent high-frequency fluctuations in the infrasonic range (i.e., <20 Hz). Though an impulsive pressure signal could be expected from a close impact event, the long duration HF pressure wave packet we observed is similar to scattered pressure signals related to explosions seen in infrasound records on Earth (Green et al., 2011). Such scatterings of acoustic energy can occur when small-scale gravity waves perturb the lower atmosphere wave guide (e.g., Damiens et al., 2017; Green et al., 2011). Nonetheless, other facts concur to put aside the impact hypothesis as a source of the observed pressure fluctuations: (1) High-frequency pressure fluctuations are recorded by InSight almost every sol in the evening, (Banfield et al., 2020); (2) acoustic propagation models (Garcia et al., 2017; Spiga et al., 2018) show that the InSight lander is in a shadow zone for infrasound waves generated at the impact location (Figure S11); and (3) owing to the noise levels of the respective instruments, if infrasound signals were seen in InSight pressure data, they would also be seen in the seismic data. They would also have to be at a significantly larger distance than this case (Martire et al., 2020). This makes it very difficult to ascribe these particular pressure fluctuations to the sol 116 seismic event or to any impact-induced phenomena at the distance of the known impact.

Regarding an airburst signal, none of the candidate events have two distinct arrivals with the expected temporal spacing of ~2 min (section 2.4), even if they were above the detection threshold, so we do not believe an impact airburst was detected for this event. To summarize, while interesting atmospheric signals were noticed during the three events, they are not likely related to either the seismic events in question or to the impact event.

4. Discussion

4.1. Reassessment of Seismic Impact Discriminators

Over the first months of the InSight mission, we have learned that marsquakes (whether sources are impact or tectonic) differ from our previous experience with either terrestrial or lunar analogs. The impact discriminators we planned on using before arriving at Mars (Daubar et al., 2018) have limited utility given the reality of Martian seismic signals recorded thus far. The marsquakes observed so far are small in amplitude, with surprisingly long durations and with apparently low attenuation/high Q. This makes many of these

characteristics difficult to distinguish. We reassess (*in italics*) each of those planned discriminators in light of real seismic data from InSight:

1. *First motion*. Impacts create positive pressure impulses, creating a positive first motion, in a direction away from the source.
   - Despite the low noise recorded by InSight during periods of the day, marsquake signals have proven to be very small. In all but the largest signals seen so far, phase arrivals are emergent, so noise obscures the direction of first arrivals. Scattering in the regolith randomizes the energy.
   - Even if we had clear first motions, quakes with a double couple source would have a positive first motion 50% of the time anyway, assuming a random orientation of sources.

2. *S wave energy*. Impacts produce more *P* waves than *S* waves.
   - A quake could also have low *S* energy for an unfavorable source orientation.
   - *S* waves are obscured by scattered *P* energy, so this is hard to determine for small events.

3. *Magnitude ratio*. Impacts produce fewer surface waves, so impacts should have a strong difference between magnitudes based on body waves and those based on surface waves.
   - Surface waves are not being detected for any Martian events (Giardini et al., 2020). The absence or diminished presence of surface wave energy, therefore, cannot be used as an impact discriminator, because all events lack surface waves.

4. *Frequency content*. Different source mechanisms lead to a smaller cutoff frequency for impacts.
   - Cutoff frequencies for the largest of the detected Martian events, where they can be determined, are typically near 6 Hz but can rise up to 12 Hz (Giardini et al., 2020). This cutoff frequency is much higher than the ~1–3 Hz expected for impacts (Daubar et al., 2018).

5. *Depth phases*. Impacts occur at the surface, implying no depth reflected phases.
   - Additional phases beyond *P* and *S* arrivals have not been identified in any events thus far (Giardini et al., 2020) because of scattering and the resulting extended codas, so a lack of depth phases cannot be used to indicate an impact.

4.2. Revised Predictions of Impact Detections by InSight

As this is the only impact known to have occurred this close to InSight during its prime science monitoring phase thus far, we wish to evaluate how likely this particular impact event was. Using an estimated current cratering rate, we can estimate the probability of a ~1 m diameter crater forming within ~50 km of InSight in one Earth year. Unfortunately, the cratering rate for impacts of this scale is not well constrained. As an estimate, we use a production function based on an extrapolation of the fragmentation model of Williams et al. (2014) pinned to the production function based on observed dated craters from Daubar et al. (2013) (see Teanby, 2015, for more details). The resulting rate is $\sim 2 \times 10^{-5}$ impacts >1 m diameter/km^2/Earth year. The uncertainty on this value is probably at least a factor of 10 in both directions. For this impact rate, the probability of one impact in any given circle of radius 50 km each Earth year is ~0.2. Thus, this event is not completely unlikely, but we were quite lucky to catch it in the images, which have covered only a small fraction of that area multiple times since Insight landed.

Based on measured noise levels of SEIS on the ground at Mars, we can revise our prelanding estimates of the number and size of impact detections to expect during the InSight mission. Teanby and Wookey (2011) and Teanby (2015) estimated seismic impact detection rates with predicted Mars seismic noise. We can now update these predictions using measured noise levels from the first few months of InSight operations. Teanby and Wookey (2011) model results for large impacts predict their peak seismic energy will be in the 1–2 Hz frequency range (where the SEIS-VBB instrument is most sensitive). Teanby (2015) compiled observations from small impacts and explosions to suggest that their peak seismic energy will be in the 1–8 Hz frequency range (where the SEIS-SP instrument is most sensitive). Typical SEIS noise levels are 0.3–

10×10^{-9} m/s^2/Hz$^{1/2}$ in the 1–8 Hz range (Lognonné et al., 2020), although during much of the Martian day SEIS sees considerably higher noise than these levels. Using scaling relationships developed in previous work (Teanby, 2015; Teanby & Wookey, 2011), we can predict *P* wave amplitudes for different size impacts at various distances (Figure 2). To get the expected frequency of impacts of different sizes, we use the production function developed by Teanby (2015) that uses new dated craters from Daubar et al. (2013) extrapolated to smaller diameters to account for the observational rollover using the Williams et al. (2014) fragmentation model. As signals at the noise level are very difficult to detect (as demonstrated by this paper!), we use a more conservative restriction of SNR ~ 3 to be realistic. InSight's noise measurements show that the Martian day can be roughly split into low-noise and high-noise time periods. Assuming a typical low noise level of 1.5×10^{-9} m/s^2/Hz$^{1/2}$ at 4 Hz (Lognonné et al., 2020) is appropriate approximately 50% of the time, and the remaining 50% of the time it is too noisy for any detections, we predict just ~2 detections of impact events per Earth year, during times when higher continuous rate data are collected. Furthermore, seismic amplitudes of signals from small craters could be even lower (Wójcicka et al., 2020) resulting in even fewer detections. There are still large uncertainties on the predicted detection rate, at least an order of magnitude. However, given that we have yet to unambiguously detect any impacts in the seismic data, either the large end of this range is increasingly unlikely, or—more likely—we have not yet learned enough about Martian seismic signals to recognize impacts in the data.

Because of this revised expectation of seismic detections of impacts, we have reversed our operational approach to detecting impacts. Instead of examining the seismic data for possible impact-induced signals, then following up with orbital images appropriate for the expected size and location of the impact, as described in Daubar et al. (2018), we are instead examining orbital images for new impacts, as indicated by dark spots or albedo changes near InSight. When more of these are found, we will examine the seismic data during the image-constrained time periods in a manner similar to the analysis presented here.

5. Conclusions

The exciting and lucky observation of a new impact occurring very close to the InSight lander during its prime mission presented a first opportunity to test our understanding of the seismic detectability of small impacts on Mars. Three potential candidate events were identified in the seismic data during the time period constrained by the before and after orbital CTX images; however, we are not able to determine that any of those seismic or atmospheric signals were definitively associated with that impact event. This is mainly because although the impact was nearby, it was quite small, forming only a ~1.5 m diameter crater, and likely was created by a significantly decelerated impactor. We predict that the signals produced by this impact were very close to the measured minimum noise amplitudes seen by the InSight seismometers, and for a good portion of the time, the observed noise levels are well above the predicted impact signal amplitude. Thus, a lack of detection for an impact of this size and at this location is disappointing, but not surprising.

There are many uncertainties in our predictions of seismic signals from the known impact, for example, in converting crater size to seismic moment. The attenuation and scattering properties of the Martian crust are not yet completely understood nor is the velocity structure of the subsurface. Given the uncertainties in our predictions, it is still possible that the known crater was indeed responsible for one of the three candidate seismic events, although we cannot support that conclusion with our current knowledge. As InSight reveals more about the properties of the Martian interior, the uncertainties in our predictions will be reduced. Future efforts at numerical modeling of this specific impact and coupled seismic modeling of the resulting wave propagation may reveal additional things to look for in the seismic or atmospheric data that may allow us to identify future impacts, if not this particular event. As we did not positively detect this impact in the data, we can at least conclude that we are not grossly underestimating the seismic amplitudes from impact events. Likewise, we see no definitive signals associated with this impact in the atmospheric data, nor do we expect that would be likely in this specific case.

The process of searching within the continuous seismic data from InSight for evidence of an event associated with an image-constrained impact has refined our understanding of impact-generated seismic signals through forward modeling and allowed us to reevaluate our predictions of impact detectability. Using the now-known noise levels of the SEIS instrument on Mars, we expect ~2 impact detections with SNR > 3

each Earth year. This is assuming continued high sampling rates able to detect higher frequency peaks, which have lately begun. Our continued efforts to search orbital images for new dated impacts near InSight will almost certainly result in more image-constrained impacts. This work has provided a template workflow to help us quickly identify future impact seismic signals associated with image-detected craters. We continue to listen for impacts on Mars.

Data Availability Statement

All data used in this work are publicly available via the Planetary Data System (https://pds.nasa.gov/). Specifically, CTX images can be found at https://pds-imaging.jpl.nasa.gov/volumes/mro.html, HiRISE images can be found at https://www.uahirise.org/, and InSight APSS/TWINS/PS data can be found at https://atmos.nmsu.edu/data_and_services/atmospheres_data/INSIGHT/insight.html website. InSight SEIS data is available in the form of a seismic event catalogue (https://doi.org/10.12686/a6) and waveform data (https://doi.org/10.18715/SEIS.INSIGHT.XB_2016) that are publicly available from the IPGP Datacenter and IRIS-DMC, as well as raw data available in the PDS (https://pds-geosciences.wustl.edu/missions/insight/seis.htm). Apollo seismic data are available in raw form at https://darts.isas.jaxa.jp/planet/seismology/apollo/index.html, and the data are available in SEED format from the IPGP Data Center for lunar data (Code XA, http://datacenter.ipgp.fr/data.php). Seismic modeling results and parameters are available on the IPGP data center (https://doi.org/10.18715/jgr_newcratermod_2020).

Acknowledgments

We thank the CTX and HiRISE operations teams for the initial identification of the site and careful and timely acquisition of the images used to make this discovery. We acknowledge NASA, CNES, their partner agencies and Institutions (UKSA, SSO, DLR, JPL, IPGP-CNRS, ETHZ, IC, and MPS-MPG), and the flight operations team at JPL, SISMOC, MSDS, IRIS-DMC, and PDS for acquiring and providing InSight data, including SEED SEIS data. We thank two anonymous reviewers for their constructive input. I. J.D. is supported by NASA InSight Participating Scientist grant 80NM0018F0612. N.A.T., J.W., and A. H. are supported by UK Space Agency grant ST/R002096/1. The French Team acknowledge the French Space Agency CNES and ANR (ANR-14-CE36-0012-02 and ANR-19-CE31-0008-08). The Swiss co-authors were jointly funded by (1) Swiss National Science Foundation and French Agence Nationale de la Recherche (SNF-ANR project 157133 Seismology on Mars), (2) Swiss State Secretariat for Education, Research and Innovation (SEFRI project MarsQuake Service-Preparatory Phase), and (3) ETH Research grant ETH-06 17-02. G.S. C. and N.W. are supported by STFC grants ST/S000615/1 and ST/S001514/1. K.M. and A.R. are fully supported by the Australian Research Council (DP180100661 and DE180100584). A part of the 3-D simulations in the supporting information was performed on the Earth Simulator of the Japan Agency for Marine-Earth Science and Technology, another part on resources provided by the Los Alamos National Laboratory Computing Program supported by DOE. A portion of this research was carried out at the Jet Propulsion Laboratory, California Institute of Technology, under a contract with the National Aeronautics and Space Administration. This is InSight contribution number 104 and IPGP contribution 4152.

References

Banfield, D., Spiga, A., Newman, C., Forget, F., Lemmon, M., Lorenz, R., et al. (2020). First results from InSight's meteorology station on Mars. *Nature Geoscience*, *13*(3), 190–198. https://doi.org/10.1038/s41561-020-0534-0

Clinton, J., Giardini, D., Böse, M., Ceylan, S., van Driel, M., Euchner, F., et al. (2018). The Marsquake service: Securing daily analysis of SEIS data and building the Martian seismicity catalogue for InSight. *Space Science Reviews*, *214*(8), 133. https://doi.org/10.1007/s11214-018-0567-5

Damiens, F., Millet, C., & Lott, F. (2017). An investigation of infrasound propagation over mountain ranges. *Journal of the Acoustical Society of America*, *143*(1), 563–574.

Daubar, I., Lognonné, P., Teanby, N. A., Miljkovic, K., Stevanović, J., Vaubaillon, J., et al. (2018). Impact-seismic investigations of the InSight mission. *Space Science Reviews*, *214*(8), 132. https://doi.org/10.1007/s11214-018-0562-x

Daubar, I. J., McEwen, A. S., Byrne, S., Kennedy, M. R., & Ivanov, B. (2013). The current Martian cratering rate. *Icarus*, *225*(1), 506–516. https://doi.org/10.1016/j.icarus.2013.04.009

Daubar, I. J., Banks, M. E., Schmerr, N. C., & Golombek, M. P. (2019). Recently formed crater clusters on Mars. *Journal of Geophysical Research: Planets*, *124*, 958–969. https://doi.org/10.1029/2018JE005857

Garcia, R. F., Brissaud, Q., Rolland, L., Martin, R., Komatitsch, D., Spiga, A., et al. (2017). Finite-difference modeling of acoustic and gravity wave propagation in Mars atmosphere: Application to infrasounds emitted by meteor impacts. *Space Science Reviews*, *211*(1–4), 547–570. https://doi.org/10.1007/s11214-016-0324-6

Giardini, D., Lognonné, P., Banerdt, W. B., Pike, W. T., Christensen, U., Ceylan, S., et al. (2020). The seismicity of Mars. *Nature Geoscience*, *13*(3), 205–212. https://doi.org/10.1038/s41561-020-0539-8

Gillet, K., Margerin, L., Calvet, M., & Monnereau, M. (2017). Scattering attenuation profile of the Moon: Implications for shallow moonquakes and the structure of the megaregolith. *Physics of the Earth and Planetary Interiors*, *262*, 28–40. https://doi.org/10.1016/j.pepi.2016.11.001

Golombek, M. P., Warner, N. H., Grant, J. A., Hauber, E., Ansan, V., Weitz, C. M., et al. (2020). Geology of the InSight landing site on Mars. *Nature Communications*, *11*(1), 1014. https://doi.org/10.1038/s41467-020-14679-1

Green, D. N., Vergoz, J., Gibson, R., Le Pichon, A., & Ceranna, L. (2011). Infrasound radiated by the Gerdec and Chelopechene explosions: Propagation along unexpected paths. *Geophysical Journal International*, *185*(2), 890–910. https://doi.org/10.1111/j.1365-246X.2011.04975.x

Gudkova, T., Lognonné, P., & Gagnepain-Beyneix, J. (2011). Seismic source inversion for large impacts detected by the Apollo seismometers. *Icarus*, *211*(2), 1049–1065. https://doi.org/10.1016/j.icarus.2010.10.028

Gudkova, T. V., Lognonné, P., Miljković, K., & Gagnepain-Beyneix, J. (2015). Impact cutoff frequency—Momentum scaling law inverted from Apollo seismic data. *Earth and Planetary Science Letters*, *427*, 57–65. https://doi.org/10.1016/j.epsl.2015.06.037

Holsapple, K. A. (1993). The scaling of impact processes in planetary sciences. *Annual Review of Earth and Planetary Sciences*, *21*(1), 333–373. https://doi.org/10.1146/annurev.ea.21.050193.002001

Holsapple, K. A., & Housen, K. R. (2007). A crater and its ejecta: An interpretation of deep impact. *Icarus*, *187*(1), 345–356. https://doi.org/10.1016/j.icarus.2006.08.029

InSight Mars SEIS data Service. (2019). SEIS Raw Data, InSight Mission. IPGP, JPL, CNES, ETHZ, ICL, MPS, ISAE-Supaero, LPG, MSFC. Other/Seismic Network, https://doi.org/10.18715/SEIS.INSIGHT.XB_2016

InSight Marsquake Service. (2020). Mars seismic catalogue, InSight Mission; V1 2/1/2020. ETHZ, IPGP, JPL, ICL, ISAE-Supaero, MPS, Univ Bristol. Dataset. http://doi.org/10.12686/a6

JeongAhn, Y., & Malhotra, R. (2015). The current impact flux on Mars and its seasonal variation. *Icarus*, *262*, 140–153. https://doi.org/10.1016/j.icarus.2015.08.032

Karakostas, F., Rakoto, V., Lognonné, P., Larmat, C., Daubar, I. J., & Miljković, K. (2018). Inversion of meteor Rayleigh waves on Earth and modeling of air coupled Rayleigh waves on Mars. *Space Science Reviews*, *214*(8), 127. https://doi.org/10.1007/s11214-018-0566-6

le Feuvre, M., & Wieczorek, M. A. (2008). Nonuniform cratering of the terrestrial planets. *Icarus*, *197*(1), 291–306. https://doi.org/10.1016/j.icarus.2008.04.011

Lesage, P., Heap, M. J., & Kushnir, A. (2018). A generic model for the shallow velocity structure of volcanoes. *Journal of Volcanology and Geothermal Research*, *356*, 114–126. https://doi.org/10.1016/j.jvolgeores.2018.03.003

Lognonné, P., Banerdt, W. B., Giardini, D., Pike, W. T., Christensen, U., Laudet, P., et al. (2019). SEIS: Insight's seismic experiment for internal structure of Mars. *Space Science Reviews*, *215*(1), 12. https://doi.org/10.1007/s11214-018-0574-6

Lognonné, P., Banerdt, W. B., Pike, W. T., Giardini, D., Christensen, U., Garcia, R. F., et al. (2020). Constraints on the shallow elastic and anelastic structure of Mars from InSight seismic data. *Nature Geoscience*, *13*(3), 213–220. https://doi.org/10.1038/s41561-020-0536-y

Lognonné, P., Karakostas, F., Rolland, L., & Nishikawa, Y. (2016). Modeling of atmospheric-coupled Rayleigh waves on planets with atmosphere: From Earth observation to Mars and Venus perspectives. *The Journal of the Acoustical Society of America*, *140*(2), 1447–1468. https://doi.org/10.1121/1.4960788

Lognonné, P., Le Feuvre, M., Johnson, C. L., & Weber, R. C. (2009). Moon meteoritic seismic hum: Steady state prediction. *Journal of Geophysical Research*, *114*, E12003. https://doi.org/10.1029/2008JE003294

Malin, M. C., Bell, J. F. III, Cantor, B. A., Caplinger, M. A., Calvin, W. M., Clancy, R. T., et al. (2007). Context camera investigation on board the Mars Reconnaissance Orbiter. *Journal of Geophysical Research*, *112*, E05S04. https://doi.org/10.1029/2006JE002808

Malin, M. C., Edgett, K. S., Posiolova, L. V., McColley, S. M., Noe Dobrea, E. Z., & Dobrea, E. Z. N. (2006). Present-day impact cratering rate and contemporary gully activity on Mars. *Science*, *314*(5805), 1573–1577. https://doi.org/10.1126/science.1135156

Martire, L., Garcia, R., Rolland, L., Spiga, A., Lognonné, P., Banfield, D., et al. (2020). Martian infrasound: Numerical modeling and analysis of InSight's data. *Journal of Geophysical Research: Planets*, *125*, e2020JE006376. https://doi.org/10.1029/2020JE006376

McEwen, A. S., Eliason, E. M., Bergstrom, J. W., Bridges, N. T., Hansen, C. J., Delamere, W. A., et al. (2007). Mars Reconnaissance Orbiter's High Resolution Imaging Science Experiment (HiRISE). *Journal of Geophysical Research*, *112*, E05S02. https://doi.org/10.1029/2005JE002605

Parker, T. J., Golombek, M. P., Calef, F. J., Williams, N. R., LeMaistre, S., Folkner, W., et al. (2019). "Localization of the InSight Lander." *50th Lunar and Planetary Science Conference, Held 18–22 March, 2019 at The Woodlands, Texas. LPI Contribution No. 2132, Id.1948* 50. http://adsabs.harvard.edu/abs/2019LPI....50.1948P

ReVelle, D. O. (1976). On meteor-generated infrasound. *Journal of Geophysical Research*, *81*, 1217–1230. https://doi.org/10.1029/ja081i007p01217

Richter, C. F. (1958). *Elementary seismology* (768). San Francisco: W. H. Freeman.

Sato, H., & Korn, M. (2007). Envelope syntheses of cylindrical vector-waves in 2-D random elastic media based on the Markov approximation. *Earth, Planets and Space*, *59*(4), 209–219. https://doi.org/10.1186/BF03353097

Schmerr, N. C., Banks, M., & Daubar, I. J. (2019). The seismic signatures of recently formed impact craters on Mars. *Journal of Geophysical Research: Planets*, *124*, 3063–3081. https://doi.org/10.1029/2019JE006044

Schmidt, R.M., Housen, K.R. (1987). Some recent advances in the scaling of impact and explosion cratering. International journal of impact engineering, hypervelocity impact proceedings of the 1986 symposium 5, 543–560. https://doi.org/10.1016/0734-743X(87)90069-8

Shishkin, N. I. (2007). Seismic efficiency of a contact explosion and a high-velocity impact. *Journal of Applied Mechanics and Technical Physics*, *48*(2), 145–152. https://doi.org/10.1007/s10808-007-0019-6

Smrekar, S. E., Lognonné, P., Tilman, S., Bruce Banerdt, W., Breuer, D., Christensen, U., Dehant, V., et al. (2019). Pre-mission InSights on the interior of Mars. *Space Science Reviews*, *215*(1), 3. https://doi.org/10.1007/s11214-018-0563-9

Spiga, A., Banfield, D., Teanby, N. A., Forget, F., Lucas, A., Kenda, B., Manfredi, J. A. R., et al. (2018). Atmospheric science with InSight. *Space Science Reviews. Springer Netherlands.*, *214*(7), 109. https://doi.org/10.1007/s11214-018-0543-0

Stevanović, J., Teanby, N. A., Wookey, J., Selby, N., Daubar, I. J., Vaubaillon, J., & Garcia, R. (2017). Bolide airbursts as a seismic source for the 2018 Mars InSight mission. *Space Science Reviews*, *211*(1–4), 525–545. https://doi.org/10.1007/s11214-016-0327-3

Teanby, N. A. (2015). Predicted detection rates of regional-scale meteorite impacts on Mars with the InSight short-period seismometer. *Icarus*, *256*, 49–62. https://doi.org/10.1016/j.icarus.2015.04.012

Teanby, N. A., & Wookey, J. (2011). Seismic detection of meteorite impacts on Mars. *Physics of the Earth and Planetary Interiors*, *186*(1–2), 70–80. https://doi.org/10.1016/j.pepi.2011.03.004

Williams, J. P., Pathare, A. V., & Aharonson, O. (2014). The production of small primary craters on Mars and the Moon. *Icarus*, *235*, 23–36. https://doi.org/10.1016/j.icarus.2014.03.011

Wójcicka, N., Collins, G.S., Bastow, I.D., Teanby, N.A., Miljković, K., Rajšić, A., et al. (2020). The seismic moment and seismic efficiency of small1impacts on Mars. JGR Planets, submitted this issue.

References From the Supporting Information

Komatitsch, D., & Tromp, J. (2002). Spectral-element simulations of global seismic wave propagation—I. Validation. *Geophysical Journal International*, *149*(2), 390–412. https://doi.org/10.1046/j.1365-246X.2002.01653.x

Maeda, T., Takemura, S., & Furumura, T. (2017). OpenSWPC: An open-source integrated parallel simulation code for modeling seismic wave propagation in 3D heterogeneous viscoelastic media. *Earth, Planets and Space*, *69*(1), 102.

McMullan, S., & Collins, G. S. (2019). Uncertainty quantification in continuous fragmentation airburst models. *Icarus*, *327*, 19–35. https://doi.org/10.1016/j.icarus.2019.02.013

Moore, H. J. (1976) Missile impact craters (WSPR, New Mexico) and applications to lunar research, Geological Survey Professional Paper 812-B, (contributions to Astrogeology).

Nissen-Meyer, T., Driel, M. V., Stähler, S., Hosseini, K., Hempel, S., Auer, L., et al. (2014). AxiSEM: Broadband 3-D seismic wavefields in axisymmetric media. *Solid Earth*, *1*, 425–445.

Plescia, J. B., Robinson, M. S., Wagner, R., & Baldridge, R. (2016). Ranger and Apollo S-IVB spacecraft impact craters. *Planetary and Space Science*, *124*, 15–35. https://doi.org/10.1016/j.pss.2016.01.002

Rivoldini, A., van Hoolst, T., Verhoeven, O., Mocquet, A., & Dehant, V. (2011). Geodesy constraints on the interior structure and composition of Mars. *Icarus*, *213*(2), 451–472. https://doi.org/10.1016/j.icarus.2011.03.024